SUPPLEMENTAL INFORMATION

Folate Conjugated Nanomedicines for Selective Inhibition of mTOR Signaling in Polycystic Kidneys at Clinically Relevant Doses

Rajasekharreddy Pala[1], Ayan K. Barui[1], Ashraf M. Mohieldin[1], Jing Zhou[2], Surya M. Nauli[1]

[1]Department of Biomedical and Pharmaceutical Sciences, Chapman University, Irvine, CA 92618
[2]Department of Medicine, Harvard Medical School, Boston, MA 02115

Corresponding Authors

Rajasekharreddy Pala, PhD
Chapman University
9401 Jeronimo Road.
Irvine, CA 92618-1908

Tel: 714-516-5462
Fax: 714-516-5481
Email: rajasekharreddypala.bio@gmail.com; marlinbiopharma@gmail.com

Surya Nauli, PhD
Chapman University
9401 Jeronimo Road.
Irvine, CA 92618-1908

Tel: 714-516-5480
Fax: 714-516-5481
Email: nauli@chapman.edu; snauli@uci.edu

Supplemental Data

Supplement Figure 1a

a. **Preparation of PLGA-PEG-Folate**

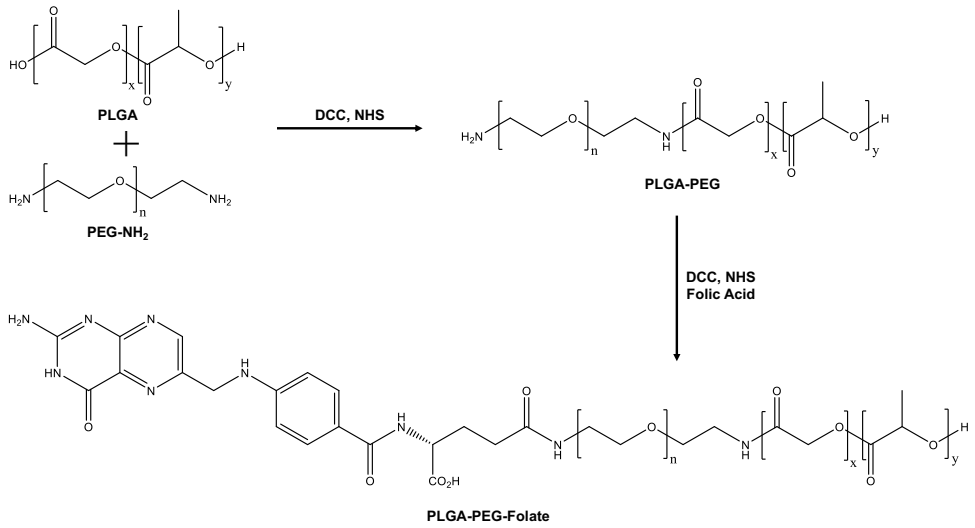

Supplement Figure 1b

b.

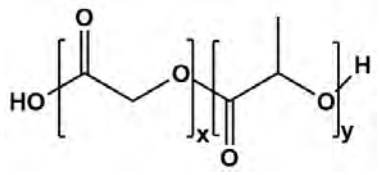

PLGA

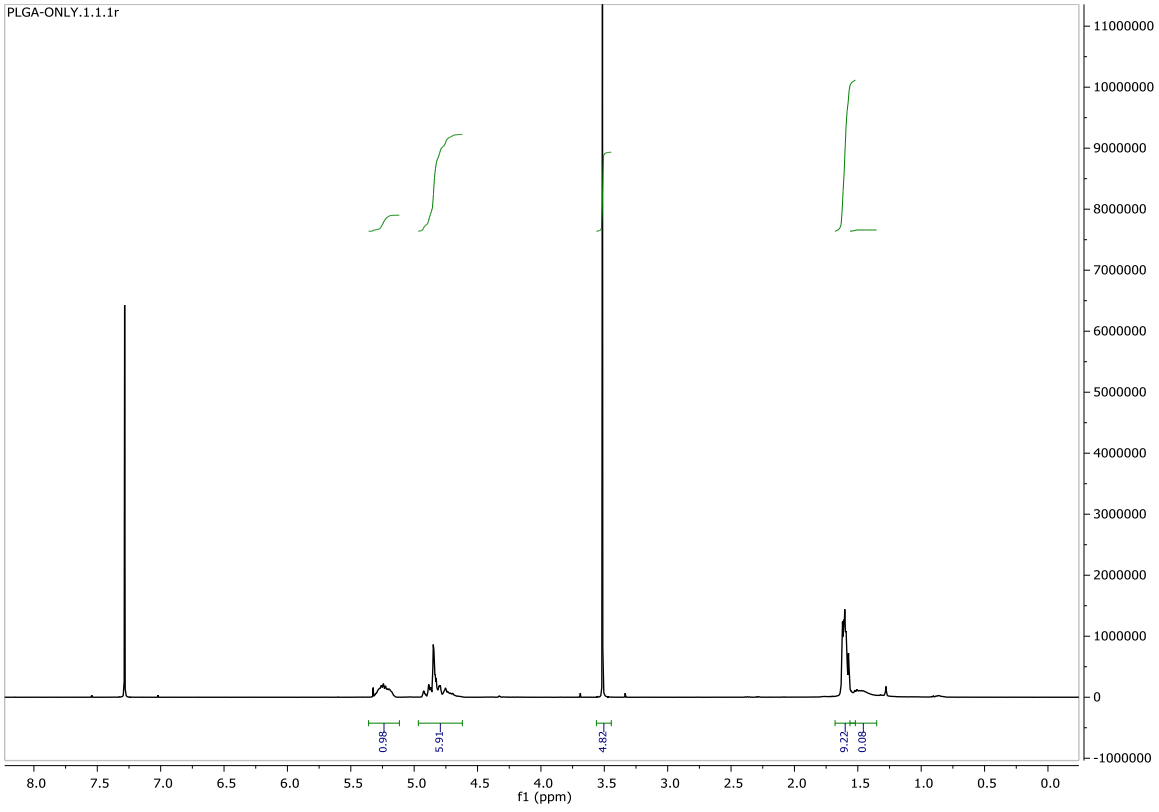

Supplement Figure 1c

c.

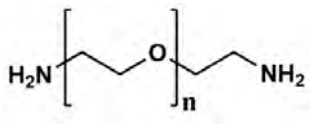

PEG

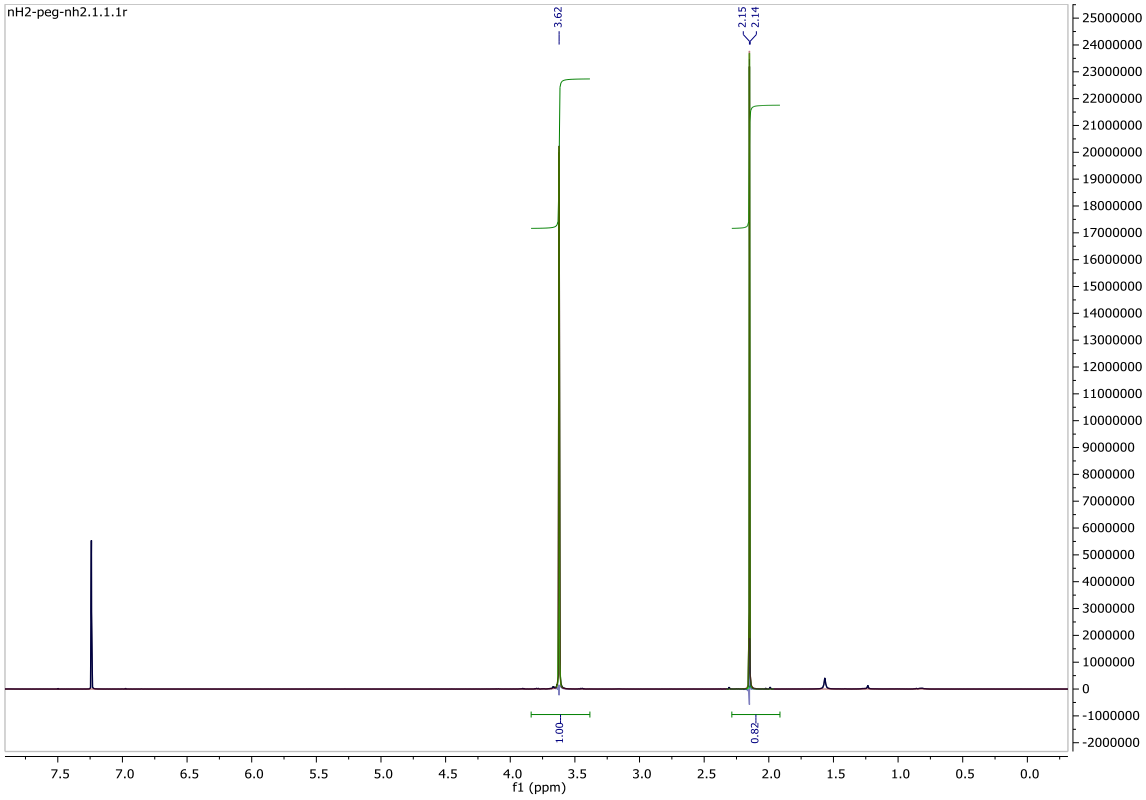

Supplement Figure 1d

d.

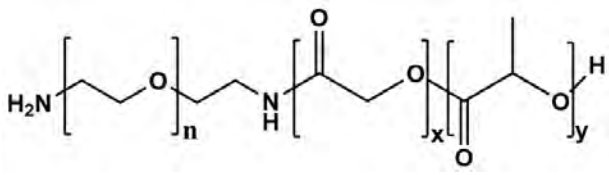

PLGA-PEG

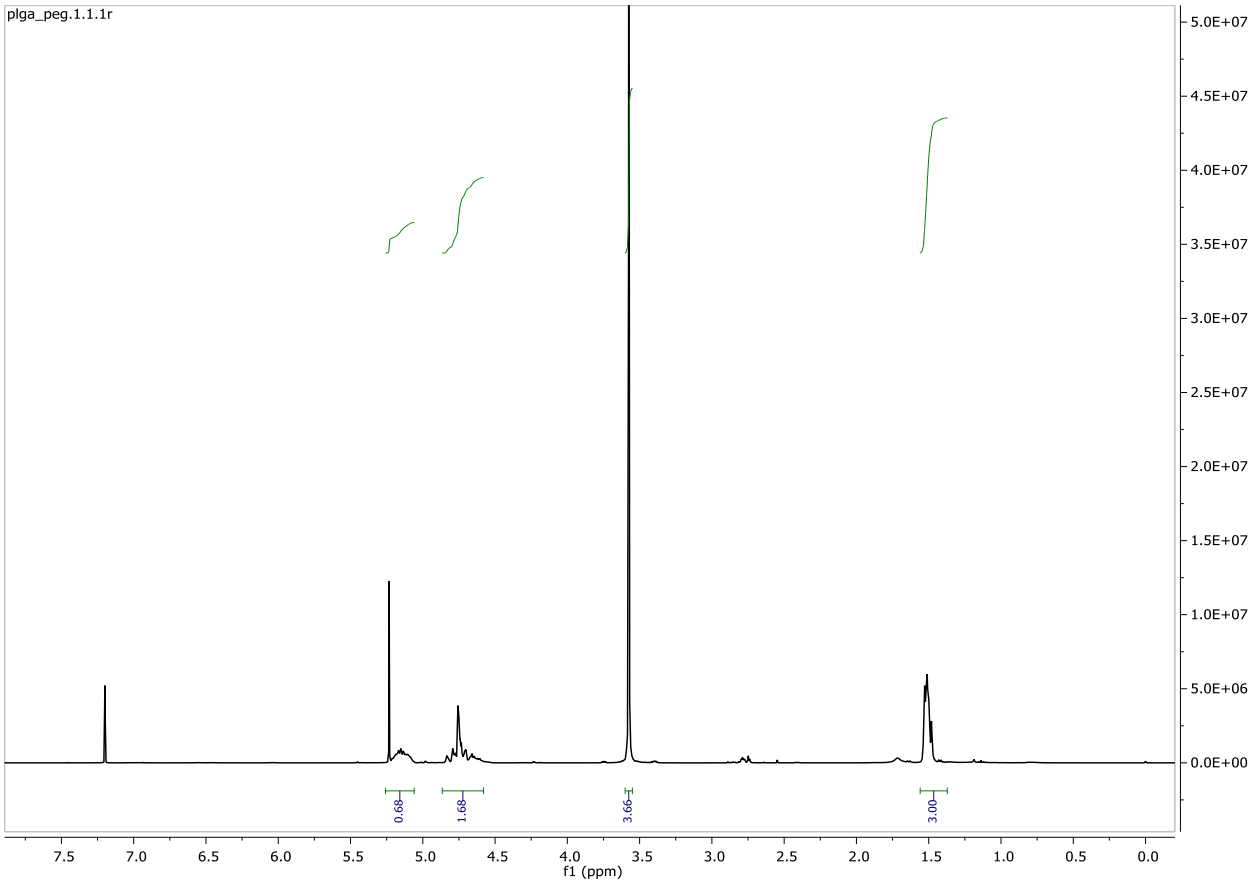

Supplement Figure 1e

e.

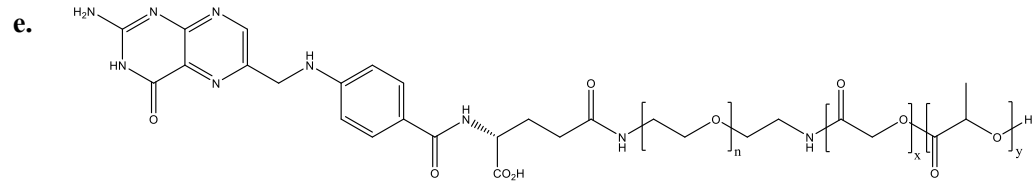

PLGA-PEG-Folate

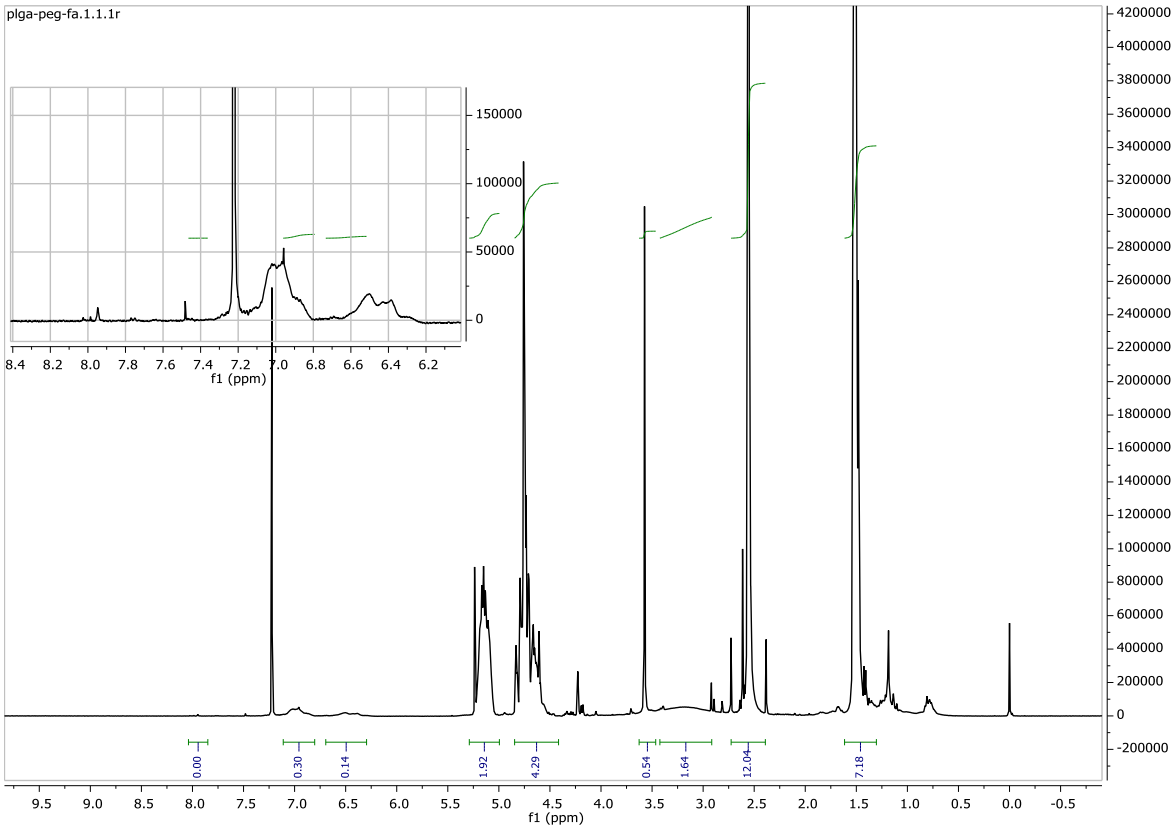

Supplement Figure 1.

a. A schematic of PLGA-PEG-Folate nanoparticle synthesis is shown.

b-e. The ^{1}H NMR spectra represent critical clues about the molecular structures, which are correspond to the proton positions in PLGA (**b**), PEG (**c**), PLGA-PEG (**d**) and PLGA-PEG-Folate (**e**). The ^{1}H NMR spectra provide chemical equivalent and non-equivalent protons. The x-axis (f1 in ppm) shows chemical shift or resonance frequency of the protons. In most cases, protons in C-H bond has a lower resonance frequency if there is no other functional groups nearby. The green integration lines on the NMR spectra represent the integration number or the relative ratio of the number of protons. The insert in NMR spectra (**e**) shows signal splitting or expansions of individual signals, so that the complex signal splitting patterns are recognizable.

Supplement Figure 2

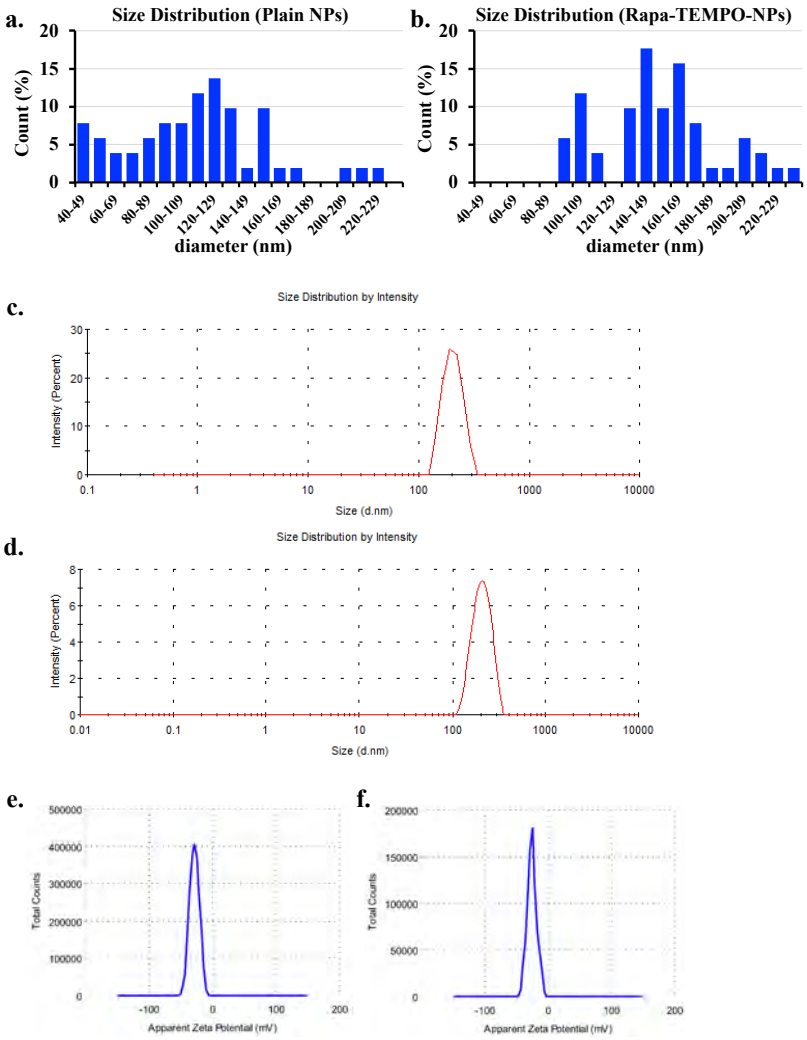

Supplement Figure 2.

a. Size distribution analysis using SEM images for plain (unloaded) PLGA nanoparticles showed NPs averaged diameter of 114 nm.

b. Size distribution analysis using SEM images for rapamycin-TEMPO-loaded PLGA nanoparticles showed an averaged diameter of 153 nm.

c. Hydrodynamic size distribution for rapamycin-loaded NPs had a peak at 209 nm.

d. Hydrodynamic size distribution for TEMPO-loaded NPs had a peak at 212 nm.

e. Zeta-potential measurement for rapamycin-loaded NPs had a peak at -28.6 mV.

f. Zeta-potential measurement for TEMPO-loaded NPs had a peak at -27.8 mV.

Supplement Figure 3

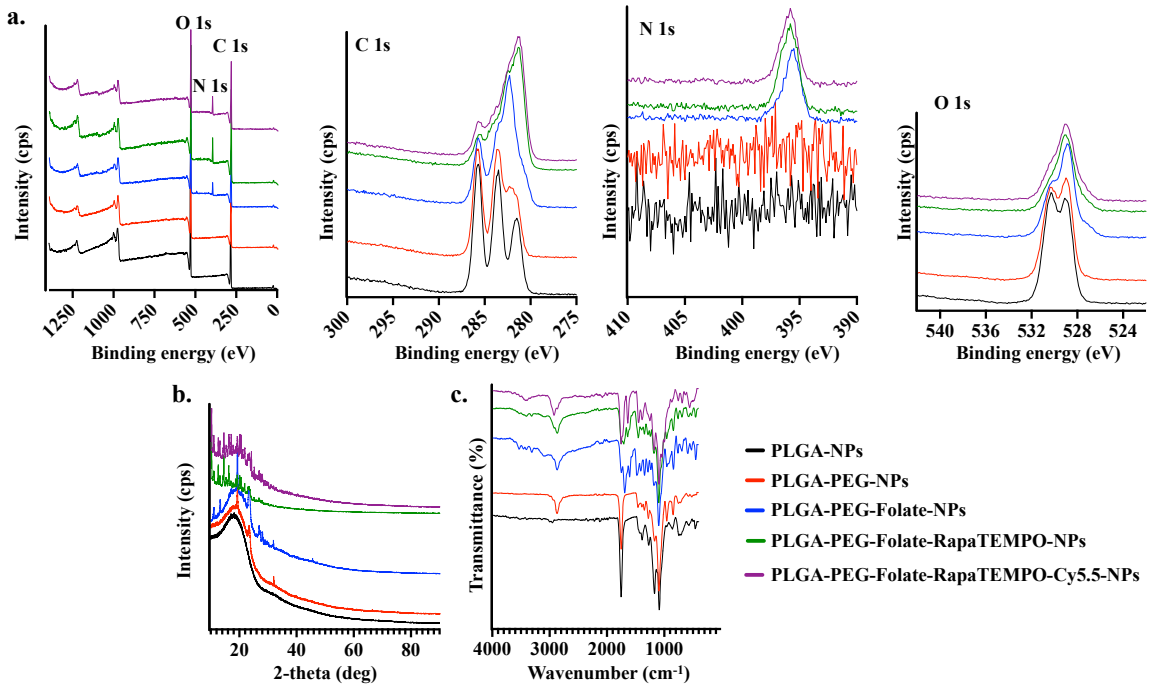

Supplement Figure 3.
Structural compositions of PLGA nanoparticles were validated and analyzed at every single major synthesis step.
a. XPS patterns of PLGA NPs are shown with different surface modifications and drug-loading. A complete spectra with several more focused survey spectra for the C 1s, N 1s and O 1s spectra are presented.
b. XRD patterns of PLGA NPs are shown with different surface modifications and drug loading.
c. FTIR spectra show the infrared signatures of PLGA NPs with different surface modifications and drug loading.

Supplement Figure 4

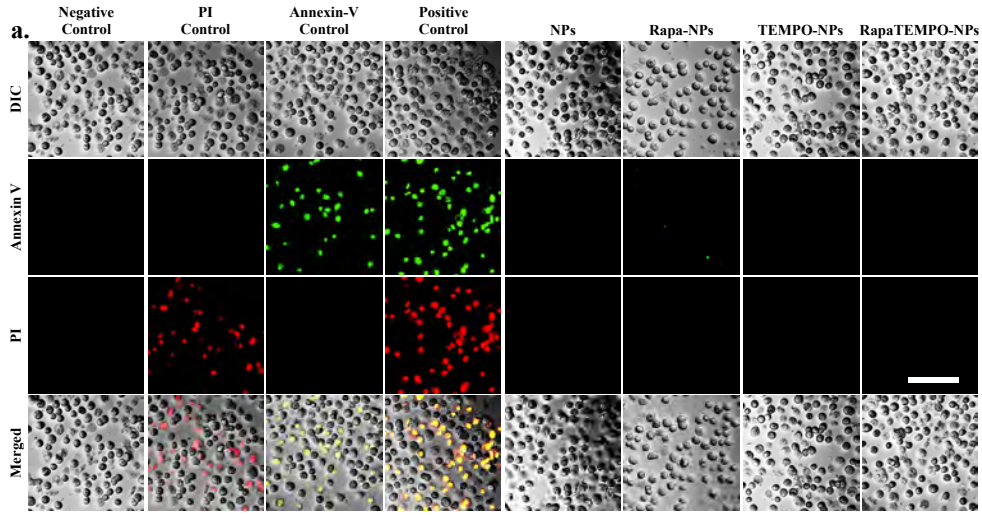

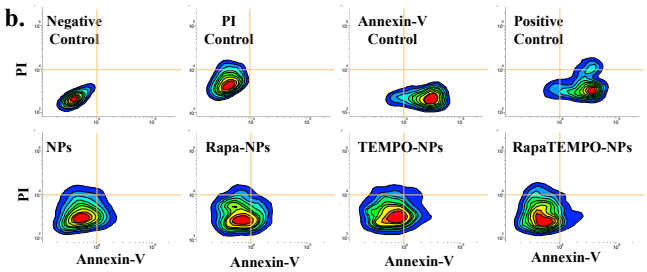

c.

	PI	Annexin-V	PI+Annexin-V	None
Negative Control	0.0±0.0	0.0±0.0	0.0±0.0	100.00±0.00
PI Control	36.54±0.34	0.0±0.0	0.0±0.0	63.41±0.38
Annexin-V Control	0.0±0.0	83.22±1.16	0.0±0.0	16.48±1.06
Positive Control	16.58±2.24	61.09±1.75	20.20±1.03	2.12±0.08
NPs	0.0±0.0	2.04±0.18	0.0±0.0	97.96±0.18
Rapa-NPs	0.0±0.0	3.48±0.32	0.0±0.0	96.52±0.32
TEMPO-NPs	0.0±0.0	2.37±0.40	0.0±0.0	97.63±0.40
RapaTempo-NPs	0.0±0.0	1.92±0.26	0.0±0.0	98.08±0.26

Supplement Figure 4.
a. Cellular toxicity of nanoparticles was visualized by DIC/fluorescence imaging. Annexin-V (green) and propidium iodide (PI; red) were used as apoptotic and necrotic markers, respectively. Scale bar=200 µm.
b-c. Toxicity was quantified with flow cytometry analysis. Data are tabulated after NP treatment for 48 hours. Negative control (no staining); positive controls (30 min-methanol permeabilization) were stained with PI-only, annexing-V-only or both annexin-V/PI.
N=3 for each group.

Supplement Figure 5

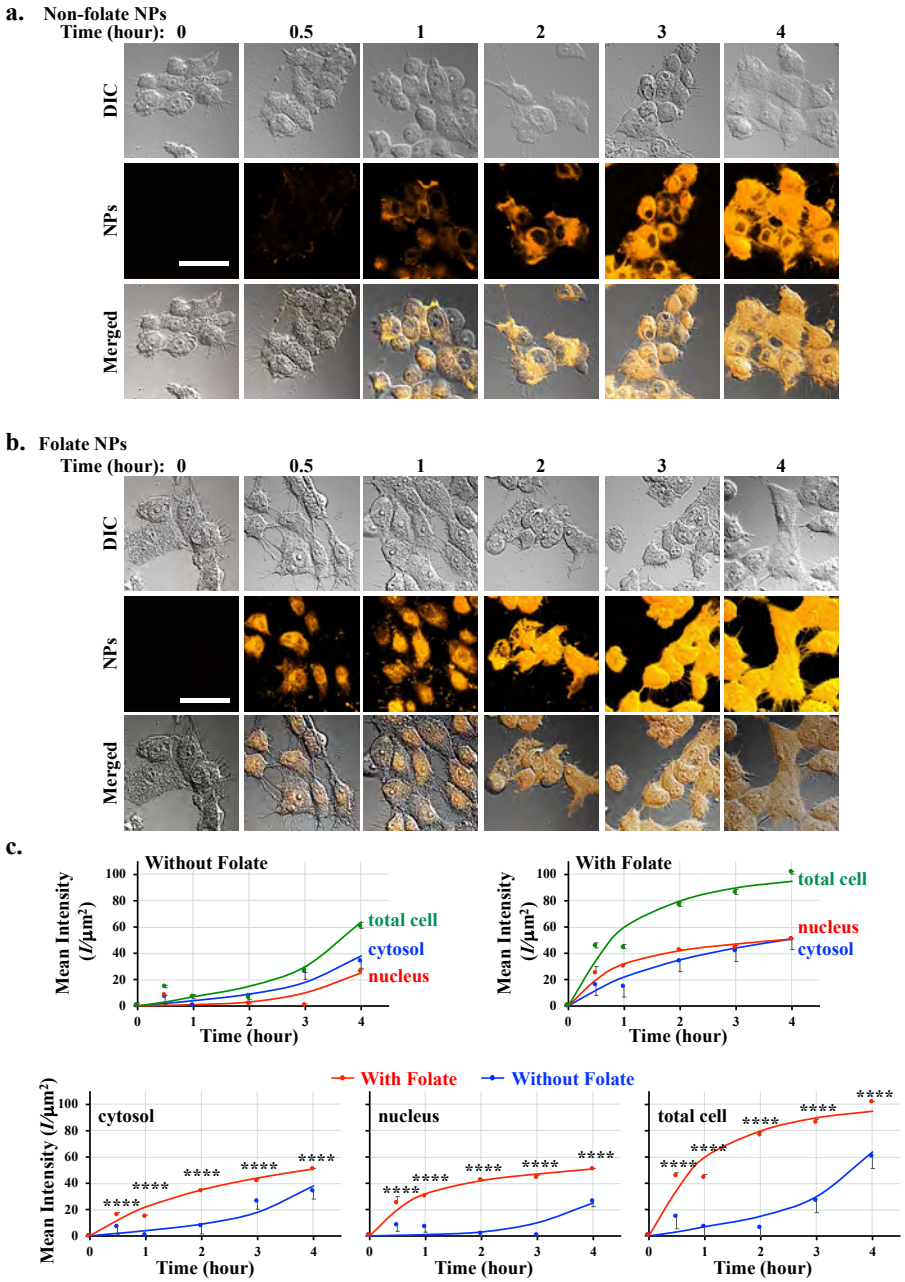

Supplement Figure 5.
a-b. Renal epithelia were treated for 4 hours with either unconjugated NPs (**a**, non-folate NPs) or folate-conjugated NPs (**b**, folate NPs). Differential interference contrast (DIC) to indicate the cells; Cy5 fluorescence to show the cellular uptake of NPs. Scale bar=100 μm.
c. The fluorescence intensity ($I/\mu m^2$) in the time-dependent manner was quantified in cytosol, nucleus and the whole cell (total).
N=5 for all experiments. ****P<0.0001 compared between unconjugated and folate-conjugated NPs.

Supplement Figure 6

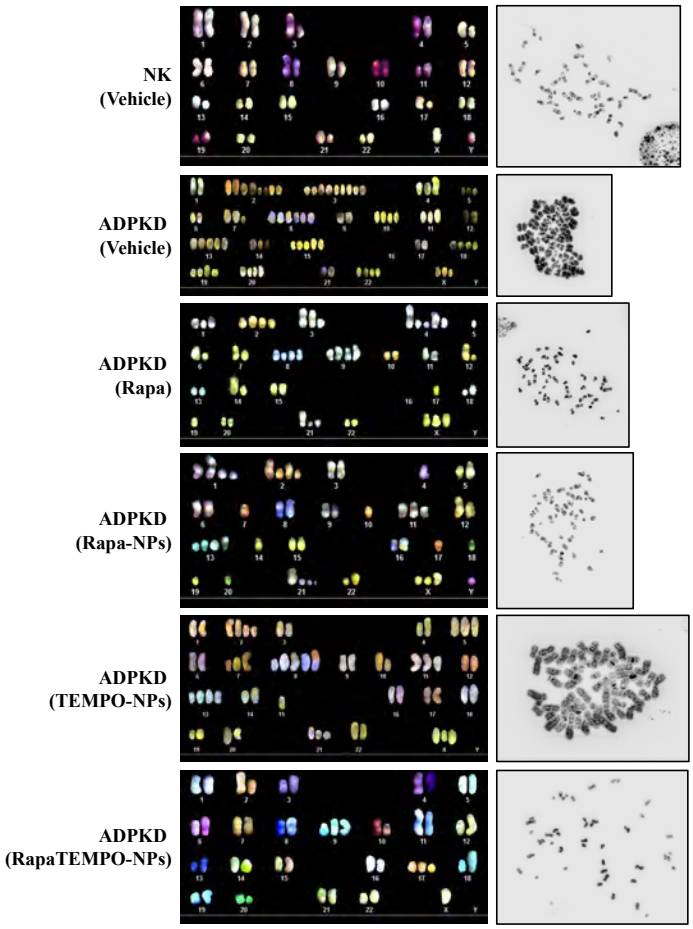

Summary	Normal	Abnormal	% Abnormal
WT (Vehicle)	11	1	8.3
Pkd2 (Vehicle)	2	10	83.3
Pkd2 (Rapa)	5	6	54.5
Pkd2 (Rapa-NPs)	4	7	63.6
Pkd2 (TEMPO-NPs)	3	8	72.7
Pkd2 (RapaTEMPO-NPs)	8	3	27.3

Supplement Figure 6.
Karyotyping analysis of human epithelial cells from normal kidney (NK) or polycystic kidney (ADPKD). Spectral karyotyping shows somatic chromosomes (1 to 22) with a pair of sex chromosomes (XY). NK cells with normal chromosome numbers and ADPKD cells with polyploidy were shown.

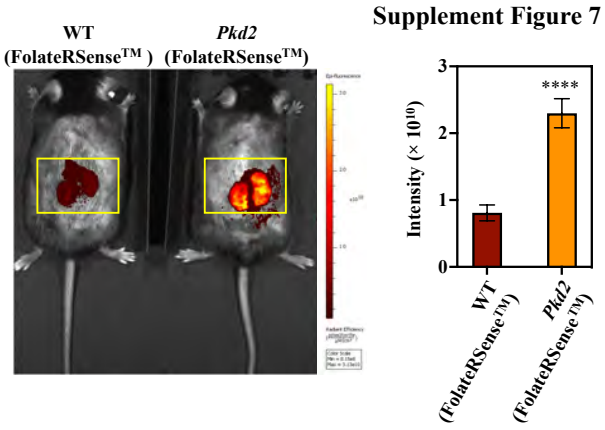

Supplement Figure 7.
Folate receptor fluorescence and their measurements were quantified in wild-type (WT) and *Pkd2* mice using renal-specific FolateRSense 680. The boxes represent the areas for quantitation. N=3. ****P<0.0001 comparing between wild-type and *Pkd2* with Student-t test.

Supplement Figure 8

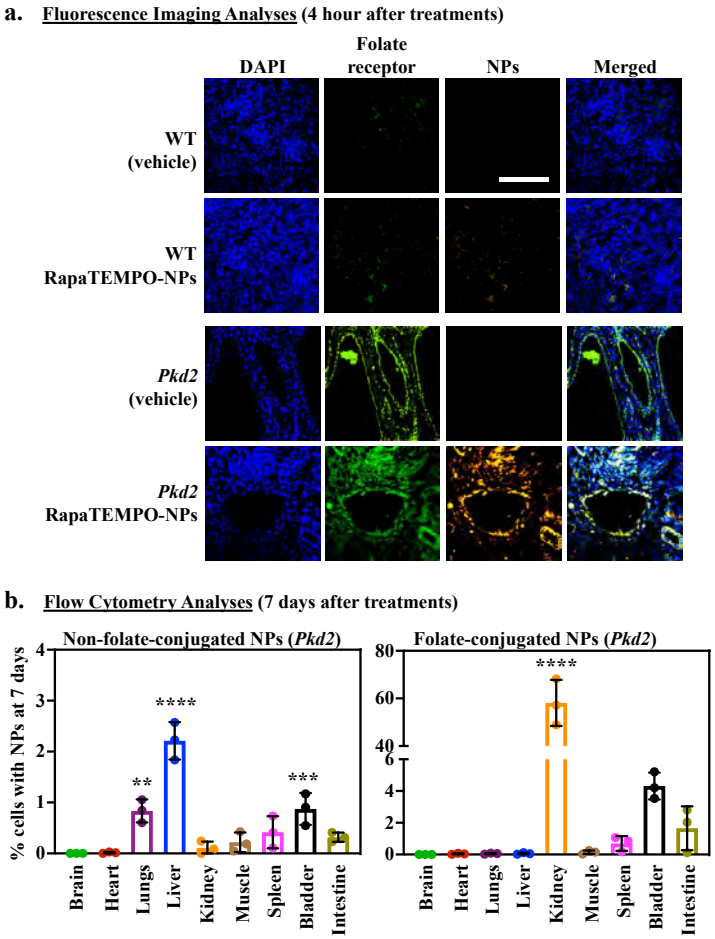

Supplement Figure 8.

a. The subcellular localizations of nanoparticles were visualized in the kidneys. Immunohisto-chemistry images show folate receptor and nanoparticle targeting in wild-type (WT) and *Pkd2* kidney sections. Folate receptor expression was greater in *Pkd2* than WT kidneys, and nanoparticles (NPs) were targeting cells that expressed folate receptor. Scale bar=500 µm.

b. In a separate study, flow cytometry analyses were carried out to validate imaging analysis in Fig.3 to determine nanoparticle distribution among all major organs. Cells from the different organs were dispersed 7 days after various treatments, and fluorescence of the nanoparticles was quantified.

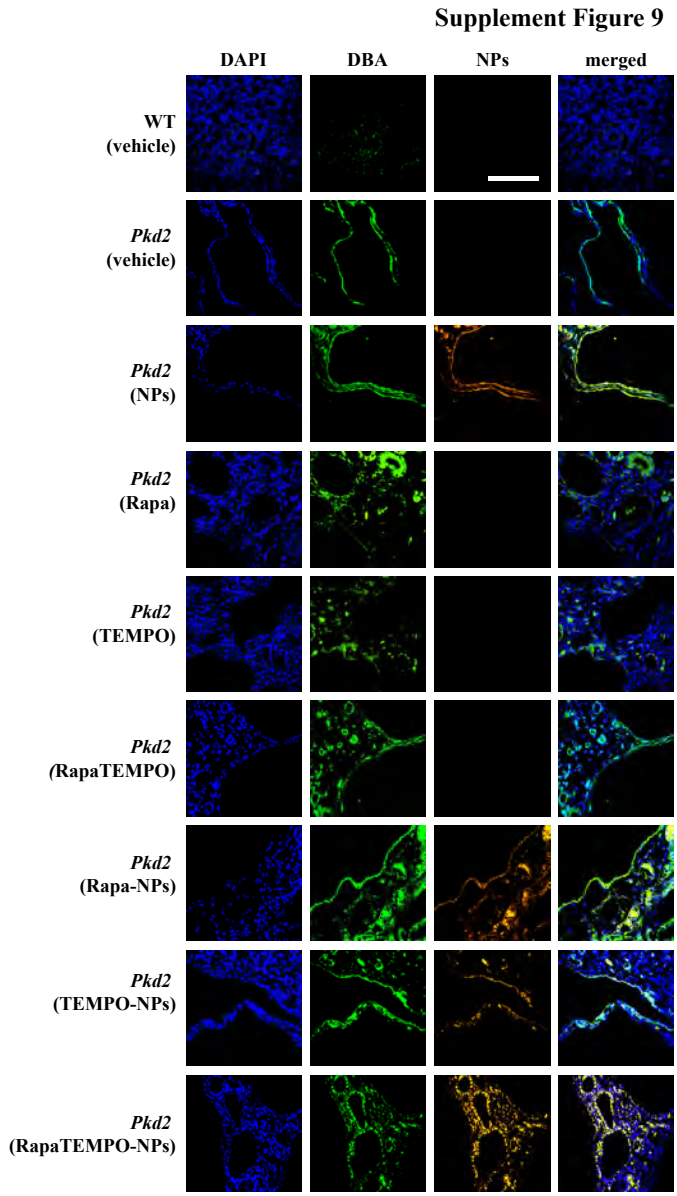

Supplement Figure 9.
Representative immunofluorescence images of mice kidney sections are shown. Blue (DAPI) stains for nucleus, green (DBA) labels the distal tubules collecting tubules, and orange represents the selective targeting of NPs to the tubules. Scale bar=500 µm.

Supplement Figure 10

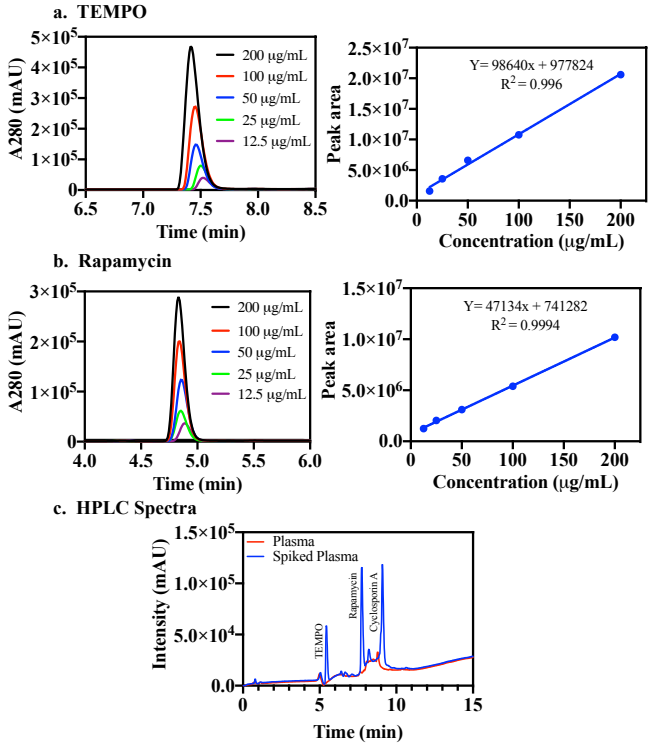

Supplement Figure 10.
a-b. The formulation and equilibration of HPLC column and liquid solvent were achieved using known rapamycin and TEMPO concentrations to obtain a standard approach and retention time. An HPLC calibration curve for both TEMPO and rapamycin (reference standards) are also shown.
c. HPLC chromatogram of plasma and plasma spiked with an internal standard (Cyclosporin A; IS), TEMPO and rapamycin is presented.

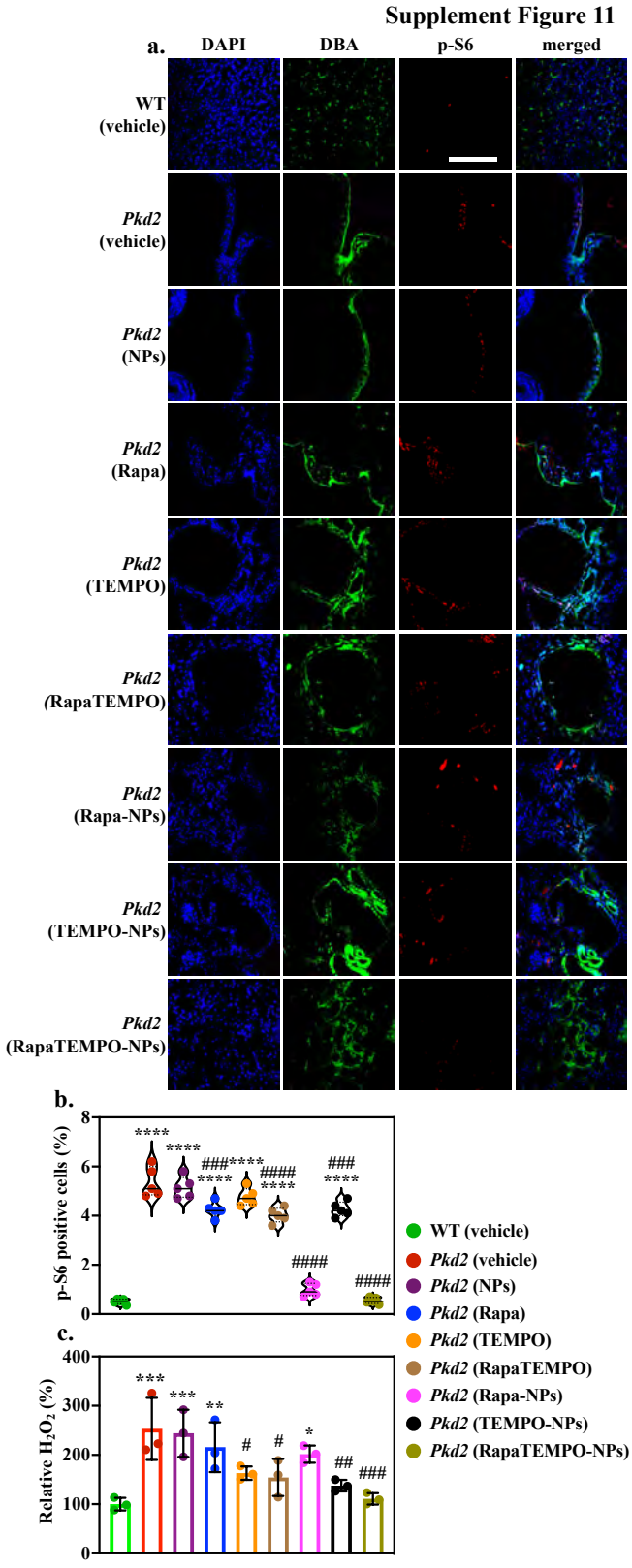

Supplement Figure 11.
To understand the roles of mTOR signaling and nanoparticles on polycystic kidneys, the central component of mTOR downstream effector phosphorylated-S6 (p-S6) was evaluated in the distal collecting tubules at the end of 9-weeks treatment.

a. Representative images show the immunofluorescence staining of phospho-ribosomal protein S6 (p-S6) in the mouse kidney sections of different groups. Scale bar=500 μm.
b. A violin plot shows the percentage of cytosolic p-S6 positive cells, normalized to the total DBA-positive nuclei in the renal tubules.
N=5 for all experiments. ****P<0.0001 compared to wild-type vehicle. ####P<0.0001 compared to *Pkd2* vehicle.

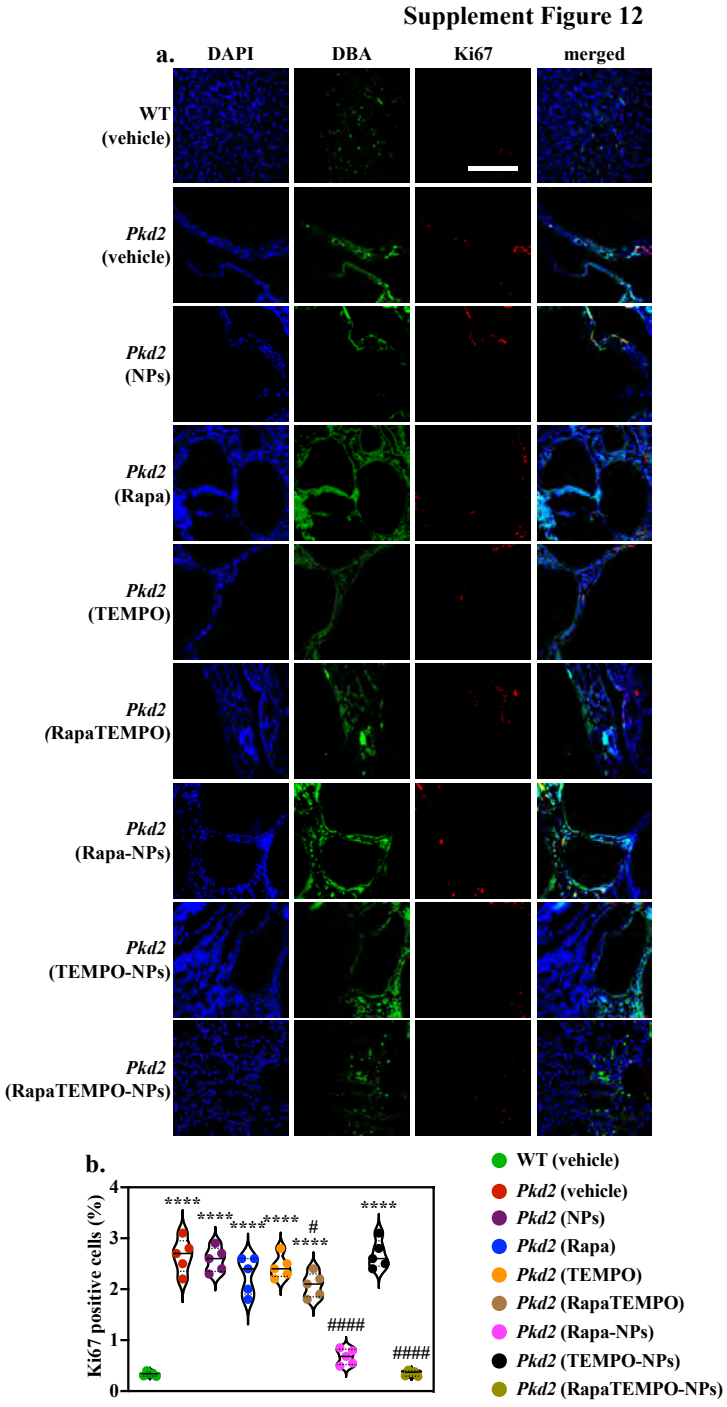

Supplement Figure 12.

To understand the effects of nanoparticles of mTOR/S6K/S6 on polycystic kidneys, proliferation index was measured in the distal collecting tubules at the end of 9-weeks treatment.

a. Representative images show the immunofluorescence staining of cell proliferation marker (Ki-67) in the mouse kidney sections of different groups. Scale bar=500 μm.

b. A violin plot shows the percentage of cytoplasmic Ki-67positive cells, normalized to the total DBA-positive nuclei in the renal tubules.

N=5 for all experiments. *P<0.05, ****P<0.0001 compared to wild-type vehicle. #P<0.05, ####P<0.0001 compared to *Pkd2* vehicle.

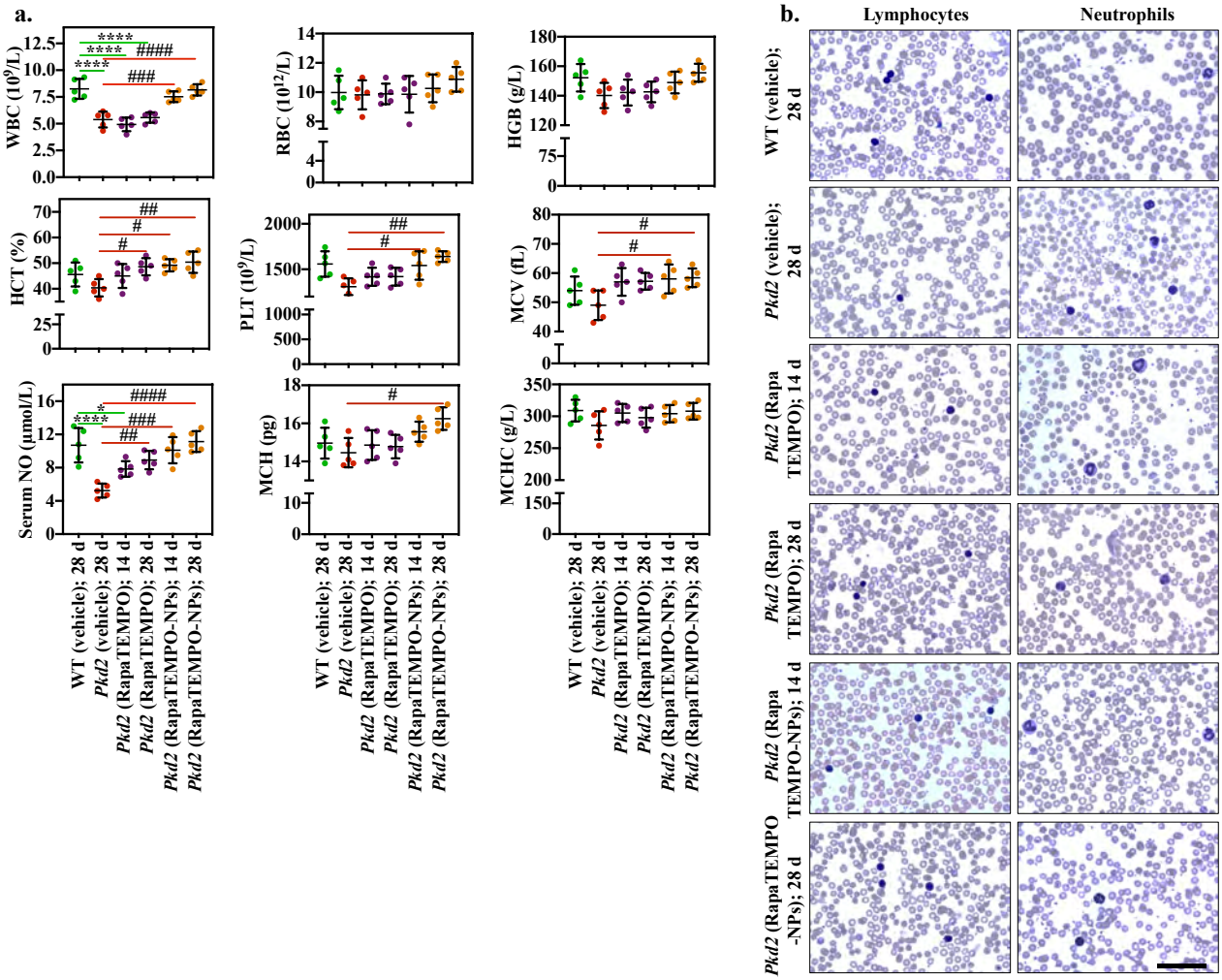

Supplement Figure 13.

The whole blood analyses were performed to screen potential side effects and immunologic responses induced by nanoparticles. These analyses were independently evaluated by a third-party, IDEXX BioAnalytics.

a. Hematology data of different treatments were analyzed for either 14 or 28 days of different treatments. Complete blood work includes white blood cells (WBC), red blood cells (RBC), hemoglobin (HGB), hematocrit (HCT), platelets (PLT), mean corpuscular volume (MCV), serum nitric oxide (NO), mean corpuscular hemoglobin (MCH) and mean corpuscular hemoglobin concentration (MCHC).

b. Wright-Giemsa staining shows the lymphocytes and neutrophils (magnification, x400) in different treatment groups for either 14 or 28 days. Scale bar=100 μm.

N=5 for all experiments. ****P<0.0001 compared to wild-type vehicle. #P<0.05, ##P<0.01, ###P<0.001, ####P<0.0001 compared to *Pkd2* vehicle.

Supplement Figure 14

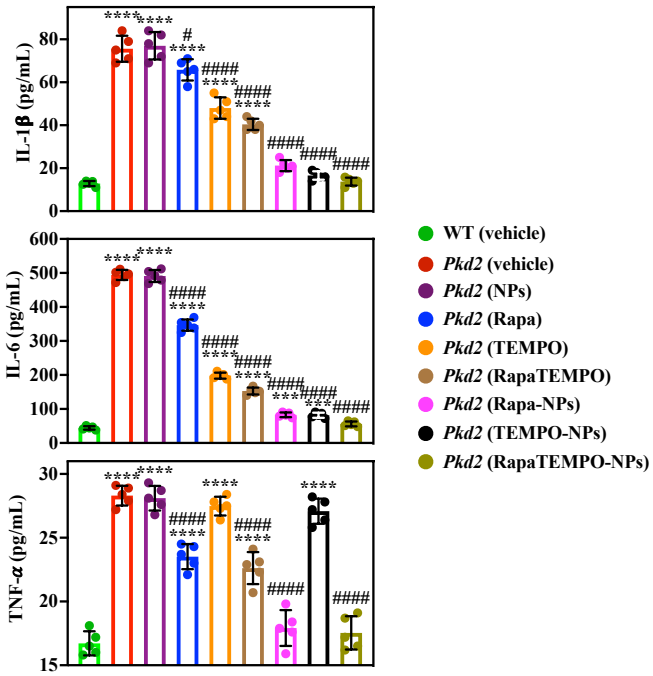

Supplement Figure 14.
Key inflammatory cytokines were studied to screen potential side effects and immunologic responses induced by the nanoparticles. The IL-1β, IL-6 and TNF-α levels from kidney supernatants were determined by ELISA and their quantifications were plotted in bar graphs, 9 weeks after treatment period.
N=5 for all experiments. *P<0.05, **P<0.01, ***P<0.001, ****P<0.0001 compared to wild-type vehicle. #P<0.05, ##P<0.01, ###P<0.001, ####P<0.0001 compared to *Pkd2* vehicle.

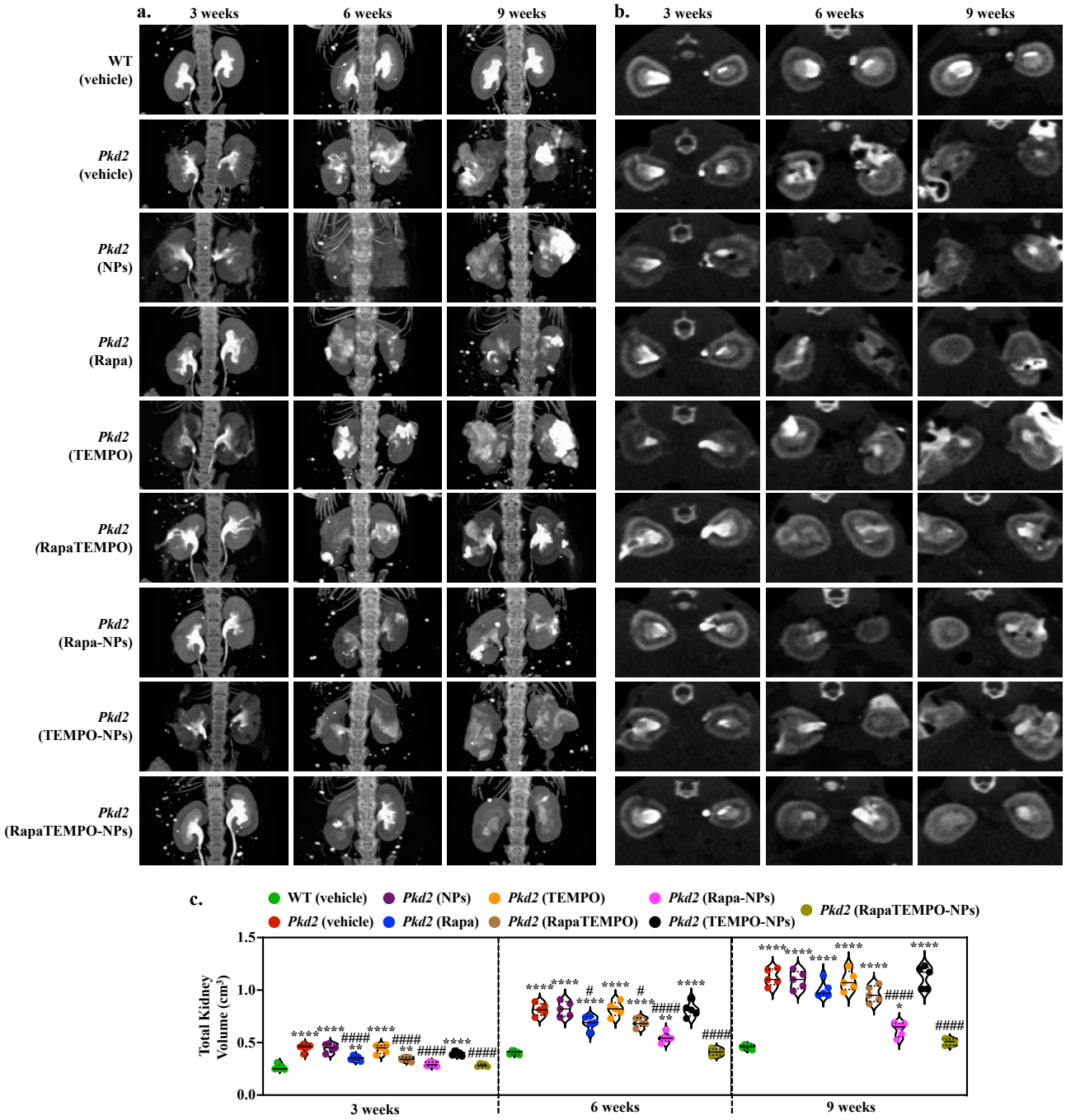

Supplement Figure 15.

Because treatments were applied prior to severe cystic development in the kidneys, computerized tomography (CT) scans were performed in the same mice during the duration of treatment to monitor progression of changes in kidney volume.

a-b. Coronal and trans-axial CT imaging of mice are shown at 3, 6, and 9 weeks of treatment time.

c. Plots show the total kidney volume at 3, 6, and 9 weeks of treatment time. The quantitative kidney volume analyses indicated that rapamycin-loaded nanoparticles had a promising effect earlier in the treatments at 3- and 6-weeks.

N=5 for all experiments. *P<0.05, **P<0.01, ***P<0.001, ****P<0.0001 compared to wild-type vehicle. #P<0.05, ##P<0.01, ###P<0.001, ####P<0.0001 compared to *Pkd2* vehicle.

Supplement Figure 16

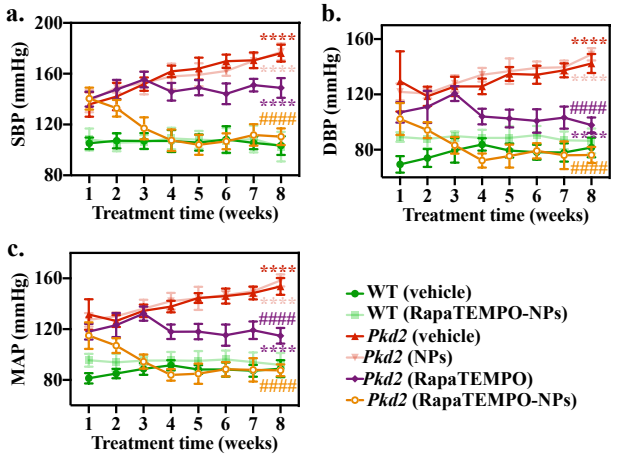

Supplement Figure 16.
To screen potential cardiac toxicities induced by the nanoparticles, key cardiac parameters were measured throughout the studies. Systolic blood pressure (**a**, SBP), diastolic blood pressure (**b**, DBP) and mean arterial pressure (**c**, MAP) for during treatment period were taken and analyzed. N=5 for all experiments. ****P<0.0001 compared to wild-type vehicle. ####P<0.0001 compared to *Pkd2* vehicle.

Supplement Figure 17

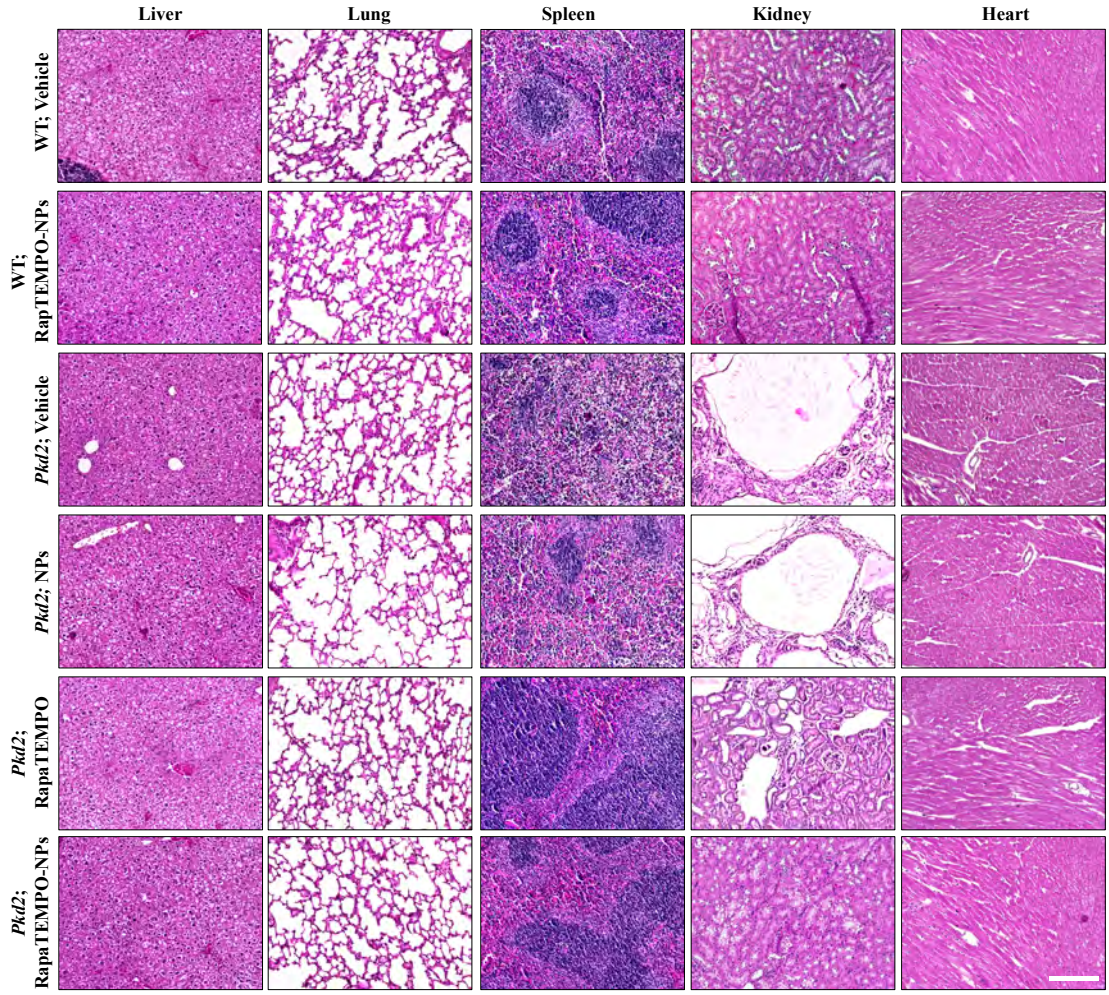

Supplement Figure 17.
To screen potential organ-specific toxicity, major organs were collected from different groups of mice at the end of the 9-week treatment. H&E staining was performed, and there was no apparent toxicity observed in all organs. Scale bar=200 μm.